Proceedings of the 11th Brazilian Congress of Thermal Sciences and Engineering – ENCIT 2006
Braz. Soc. of Mechanical Sciences and Engineering – ABCM, Curitiba, Brazil, Dec. 5-8, 2006

Paper CIT06-0578

ASYMPTOTIC PREMIXED-FLAME STRUCTURE IN A POROUS MEDIUM

Fernando Marcelo Pereira
Universidade Federal de Santa Catarina
fernando@labcet.ufsc.br

Amir A. M. Oliveira
Universidade Federal de Santa Catarina
amirol@emc.ufsc.br

Fernando Fachini Filho
Instituto de Pesquisas Espaciais
ffachini@lcp.inpe.br

Abstract. *The structure of premixed flames within porous media is investigated by using the asymptotic expansion method. The flame is divided in three distinct regions. Two of them, the gas conduction region (also known as preheating region) and the reaction region, are the same two regions present in the classical premixed flame structure. The third region is related to the heat conduction in the solid matrix. Since the chemical reaction is very sensitive to temperature, the reaction occurs in a very thin zone inside the gas conduction region, where the highest gas phase temperature is found. Also, since the solid heat conduction is higher than the gas heat conduction, the solid phase heat conduction region is much thicker than the gas phase heat conduction region. Discrepancies in the characteristic lengths among the three regions justify the application of asymptotic expansions to determine an approximated (analytical) solution. The description of the reaction region is obtained using the large activation energy asymptotic expansion and the description of the preheating region is obtained usig the boundary layer expansion. The influence of the ratio of the solid- and the gas-phasic effective conductivities, intraphasic heat transfer coefficient and the porosity of the medium are evaluated, revealing the effects of the inner flame structure on the flame stabilization within porous media.*

keywords: *combustion in porous media, asymptotic solution, superadiabatic temperature*

1. Introduction

The combustion in porous media is characterized by high temperatures in the reaction region as a result of the heat recirculation induced by the solid matrix (Howell et al., 1996). This technology has received much attention in the last decades as a way of extending flame stability, burning fuel lean mixtures and providing radiant heating. The heat recirculation induced by the porous media adds to the heat released by combustion resulting in local temperatures in excess of the adiabatic flame temperature. This has been called superadiabatic combustion (Echigo et al., 1991).

A few works have attempted to develop analytical models for the combustion in porous media. McIntosh and Prothero (1991) proposed a model for the surface combustion with radiant heat loss, i.e., for a porous burner in which the flame is stabilized on the porous medium surface or just above it. In these burners the flame is cooled by the radiant heat loss, which implies in low NOx emissions. Their work relied on the large-activation-energy asymptotic method to derive an analytical solution for the gas and solid temperatures. The solutions depend on a convective heat transfer parameter, on a radiant coefficient and on the conductivities ratio. Their results showed the effect of the parameters on the flame location and allowed for the prediction of the blow-off and flash-back conditions.

The amount of excess temperature within the porous medium depends on the thermal properties of the gas and solid phases and has been studied theoretically and numerically by Pereira and Oliveira (2005). Their analysis is based on the excess enthalpy function previously defined in the literature (Wichman and Vance, 1997) applied to the one-dimensional volume-averaged equations for the combustion within an inert porous medium. Approximations for the solid-phase temperature and fuel consumption distributions are assumed and the dependence of the excess enthalpy function on the problem parameters is analyzed.. The results obtained

are in good qualitative agreement with the numerical results but the model was not able to predict flame speeds. The excess enthalpy was shown to be a function of the gas Lewis number, the interphasic heat transfer coefficient, the ratio of the solid- and the gas-phasic effective thermal conductivities and the porosity of the medium.

Here, an asymptotic solution for an infinite, adiabatic porous burner is proposed. In contrast to McIntosh and Prothero's solution, this work focuses on adiabatic flames where superadiabatic temperatures are expected to arise. This condition is similar to that of a long, insulated burner in which the flame stabilizes deeply within the porous medium. The problem is divided in three part. The first corresponds to the problem in the solid-phase characteristic length scale. The second corresponds to the problem in the gas-phase characteristic length scale, which is about 1/40 of the solid scale. Finally, the third corresponds to the problem on the reaction region scale, which is imposed to be much thinner than the gas scale. Also, in contrast to McIntosh and Prothero's solution, the heat diffusion in the gas-phase is confined to a small part around the flame. Explicit solutions for the gas and solid temperatures and for the flame velocity are found as functions of the problem parameters. The effects of the thermal conductivities ratio, volumetric porosity and equivalence ratio on the temperature profiles and flame velocity are analyzed..

2. Length Scales

The main difference of flames within porous media when compared to freely propagating flames is the presence of the solid-phase thermally connecting the two sides of the flame. The properties of the gas and solid phases are very dissimilar; the solid-phase thermal conductivity can be several orders of magnitude larger than the gas-phase thermal conductivity, thus, the thermal diffusion is enhanced when the reaction takes place within a solid matrix. The intraphasic radiant heat transfer among solid particles plays an important role in the heat transfer from the hot to the cold regions of the flame, specially for structures with small optical thickness (Barra and Ellzey, 2004). As a consequence of these dissimilar properties and noting that the exotermic reaction occurs only in the gas-phase, the combustion in porous media is characterized by local thermal non-equilibrium between the solid and the gas phases, resulting in local interphasic heat transfer (Oliveira and Kaviany, 2001). As a consequence, the heat transport by conduction and radiation through the solid matrix preheats the incoming gas as a result of the interphasic heat transfer, in a heat recirculation process. The large interfacial surface area between the phases allows for large rates of interphasic heat transfer, which in turn results in large heat recirculation. The heat recirculated adds to the energy released by combustion resulting in temperatures above that of the adiabatic free-flame.

Consider the propagation of an adiabatic plane flame within an infinite inert porous medium as represented in Fig(1). Figure (1A) shows a rendering of the temperatures and fuel mass fraction distributions for the different characteristic length scales of the problem. The figure shows that the flame structure can be described in four levels of detail. The first level (Fig.1B) is a flame front travelling with velocity s_f against the unburnt gas. The velocity of the front in relation to a fixed reference frame is $w = u_n - s_f$, where u_n is the incoming gas velocity (for stationary flames $u_n = s_f$). Note that the Darcean flame speed, s_D, or filtration velocity, is smaller than the velocity of the fluid-phase inside the matrix ($s_D = \varepsilon\, s_f$, where ε is the volumetric porosity of the matrix). The flame front separates two regions of thermodynamic equilibrium related through mass and energy conservation. Upstream from the front, the temperatures of both phases and the fuel mass fraction are equal to their initial values, T_n and Y_{Fn} respectively. Downstream from the front, the temperatures of both phases reach the adiabatic flame temperature T_r, according to the thermodynamic requirement, and the mass fuel fraction decreases to its final value, Y_{Fr}, which is zero for understoichiometric mixtures. The thickness of the flame front is represented by l_{Ds} and can be several centimeters long (Pereira e Oliveira, 2002).

In the second level of detail (Fig.1C), the heat conduction through the solid-phase, the interphasic heat transfer and gas convection control the problem. The transport of mass and heat by diffusion in the gas-phase are collapsed in a thin region (a flame sheet). The gas-phase temperature and the fuel mass fraction are discontinuous at this interface and thermal nonequilibrium between the phases occur upstream and downstream from the flame. Upstream from the flame the unburnt gas is heated up by the solid-phase, at the flame the gas temperature reaches the superadiabatic peak, T_{sup}, and downstream from the flame, the burnt gases looses heat to the solid-phase decreasing its temperature from the maximum value to the adiabatic flame temperature. The fuel mass fraction is constant and equal to its initial value upstream from the flame and is completely consumed at the flame sheet for lean mixtures. The temperature of the solid-phase varies smoothly from T_n to T_r as a result of the thermal diffusion. The flame sheet (Fig.1C) moves against the unburnt mixture with a velocity higher than the flame velocity s_f (Fig.1B) since the gas at the flame has been preheated by the solid matrix. The thermal affected region is wider than that of a free flame as a result of the high solid thermal conductivity. This can be expressed by a modified Lewis number, Le_s, defined as $Le_s = \Gamma Le$, where Γ is the ratio of the solid and gas thermal conductivities ($\Gamma = \lambda_s/\lambda_g$) and Le is the gas Lewis number ($Le = \lambda_g/\rho\, c_p$). Since $\Gamma \gg 1$, the modified Lewis number is always greater than unity, showing that, for the combustion in porous media, the

thermal length is always greater than the mass diffusion length. The thermally affected region can be expressed by a characteristic solid-phase diffusion length scale defined as $l_{Ds} \sim (\lambda_s/\rho c_p)/u_n$.

In the third level of detail (Fig.1D), the flame is expanded revealing the mass and heat transport by diffusion in the gas-phase. In the classical description of free-flames this region is known as the preheating region. Since large activation energies are found for the major part of the fuels of interest in combustion, it is expected that the reaction will be restricted to a thin region (a reaction sheet). The reaction will be a heat source and a reactant sink in the gas-phase. Thus, near the reaction sheet the gas temperature increases due to gas-phase heat conduction and the fuel concentration decreases because of the fuel depletion towards the reaction front. The gas temperature and fuel mass fraction distributions are not linear as a result of the convection transport and their slopes change discontinuously across the reaction sheet. On the other hand, the solid-phase temperature is practically linear because the interphasic heat transfer is expected to be negligible compared to the gas conduction. Now, a characteristic gas-phase diffusion length scale can be defined as $l_{Dg} \sim (\lambda_g/\rho\, c_p)/u_n$, where diffusion and convection in the gas-phase are the controlling mechanisms.

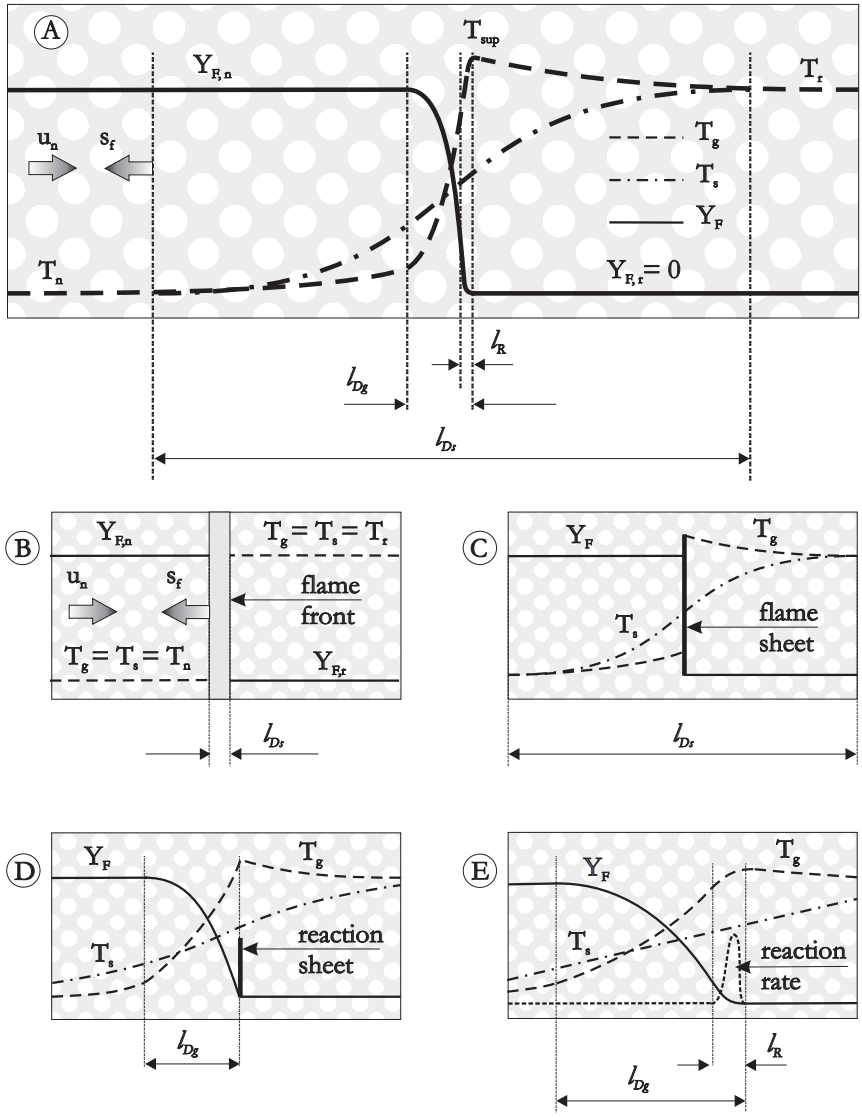

Figure 1 - Rendering of the temperatures and fuel mass fraction distributions for the different characteristic length scales of the problem.

In the last, and more complete, level of detail (Fig.1E), the reaction sheet is expanded revealing the reaction rate and the continuous variations of the gas temperature and fuel mass fraction slopes. Now we are interested in defining a characteristic reaction length scale l_R. This can be done by comparing the magnitude of the temperature change across the characteristic reaction length scale (ΔT_R) with that across the characteristic gas-phase diffusion length scale (ΔT_{Dg}): $l_R \,/\, l_{Dg} \sim \Delta T_R \,/\, \Delta T_{Dg}$. Noting that the temperature increase in the gas-phase across the preheating region is equal to the temperature increase from the initial value to the adiabatic flame temperature ($\Delta T_{Dg} = T_r - T_n$) and that the temperature variation across the reaction region can

be approximated by $\Delta T_R \sim [w/(dw/dT)]_{T_r}$, where w is the reaction rate according to the Arrhenius expression, the relation between the two characteristic length scales is

$$\frac{l_R}{l_{Dg}} \sim \frac{RTr}{Ea}\frac{Tr}{(T_r - T_n)} \sim \frac{1}{\beta}$$

where β is the Zel'dovich number and usually lies between 5 and 15 (Zel'doich et al., 1985; Liñán, 1974).

It is interesting to note that the gas-phase diffusion length scale, defined as the flame thickness for freely propagating flames, is of the order of 1mm for hydrocarbon fuels. The typical ceramic foams used as solid matrix in porous burners have pore diameters ranging from 2 to 4 mm (the exceptions are the surface burners where smaller pore diameters are used). Then, the combustion reaction is not expected to spread over several pores but to be confined to one pore. The pore walls will interfere in the reaction just close to the edges of each small tridimensional flame where they will behave as a sink of energy and radicals. Ultimately, the description of the flame structure in the flame sheet within a porous medium is very similar to that of a free flame. The main difference is that in the combustion in a porous medium we find an additional wide region (l_{Ds}) of heat exchange between the gas and solid phases leading to higher gas temperature in the preheating region. Possible wall catalytic effects and flame stretch effects are not taken into account here.

From the asymptotic point of view, the flame structure analysis follows the hypothesis that $l_R \ll l_{Dg} \ll l_{Ds}$. In the following, the conservation equations are presented, nondimensionalized and solved by asymptotic expansions taking advantage of the differences among the three length scales identified.

3. Basic Set of Equations

A one-dimensional, two-medium model for the conservation of mass, gas phase energy, solid phase energy and species is written following Sahraoui and Kaviany (1994). The mass conservation implies that $\rho_n u_n$ is constant for the one-dimensional flow with ρ_n and u_n being respectively the gas density and the gas velocity far upstream from the flame. For a steady state, stationary flame, the laminar flame speed s_f is equal to u_n. The specific heat capacity c_p, the thermal conductivities (λ_g for the gas and λ_s for the solid) and the product ρD (density times mass diffusivity) are assumed uniform along the flame. The gas and solid radiation and the dispersion effects are neglected. The pressure drop in the porous medium is assumed negligible and the momentum equation becomes trivial. The thermal conductivities and the mass diffusivity are effective properties in the respective phase (i.e., include the pore channel variable area and tortuosity effects; Kaviany, 1995).

The fuel combustion is assumed to occur following a global one-step mechanism, represented in mass variables as

$$F + \nu O_2 \rightarrow (1+\nu)P$$

where ν is the mass of oxygen per mass of fuel ratio.

The steady state, volume-averaged energy and species conservation equations (omitting for simplicity the volume-averaging notation) then become

$$\varepsilon\rho u = \varepsilon\rho_n u_n \tag{1}$$

$$\varepsilon\rho_n u_n \frac{dY_F}{dx} = \varepsilon\rho D_F \frac{d^2Y_F}{dx^2} - \varepsilon A\rho^2 Y_O Y_F \; T_g^a e^{-E/RT_g} \tag{2}$$

$$\varepsilon\rho_n u_n \frac{dY_O}{dx} = \varepsilon\rho D_O \frac{d^2Y_O}{dx^2} - \varepsilon\nu A\rho^2 Y_O Y_F \; T_g^a e^{-E/RT_g} \tag{3}$$

$$\varepsilon\rho_n u_n c_p \frac{dT_g}{dx} = \varepsilon\lambda_g \frac{d^2T_g}{dx^2} + \varepsilon Q A\rho^2 Y_O Y_F \; e^{-E/RT_g} + h_v(T_s - T_g) \tag{4}$$

$$0 = (1-\varepsilon)\lambda_s \frac{d^2T_s}{dx^2} - h_v(T_s - T_g) \tag{5}$$

where Q is the fuel mass based heat of reaction, h_v is the volumetric convection coefficient, E is the activation energy and R is the universal gas constant.

4. Nondimensionalization

Defining the nondimensional variables (Williams, 1985)

$$y_F = \frac{Y_F}{Y_{Fn}}, \quad y_O = \frac{Y_O}{Y_{On}}, \quad \theta = \frac{c_p(T-T_n)}{Y_{Fn}\ Q} = \frac{T-T_n}{T_r-T_n}, \quad z = \int_0^x \frac{u_n}{(\lambda_s/\rho_n c_p)}dx \tag{6}$$

the premixed-flame within a porous medium is described by the following conservation equations

$$\varepsilon\frac{dy_F}{dz} = \frac{\varepsilon}{Le_F\ \Gamma}\frac{d^2y_F}{dz^2} - \varepsilon\widehat{D}a\ y_O y_F \exp\{-\beta(1-\theta_g)/[1-\alpha(1-\theta_g)]\} \tag{7}$$

$$\varepsilon\frac{dy_O}{dz} = \frac{\varepsilon}{Le_O\ \Gamma}\frac{d^2y_O}{dz^2} - \varepsilon\Phi\widehat{D}a\ y_O y_F \exp\{-\beta(1-\theta_g)/[1-\alpha(1-\theta_g)]\} \tag{8}$$

$$\varepsilon\frac{d\theta_g}{dz} = \frac{\varepsilon}{\Gamma}\frac{d^2\theta_g}{dz^2} + \varepsilon\widehat{D}a\ y_O y_F \exp\{-\beta(1-\theta_g)/[1-\alpha(1-\theta_g)]\} + N(\theta_s-\theta_g) \tag{9}$$

$$0 = (1-\varepsilon)\frac{d^2\theta_s}{dz^2} - N(\theta_s-\theta_g) \tag{10}$$

where

$$\Gamma = \frac{\lambda_s}{\lambda_g}, \quad \beta = \frac{E(T_r-T_n)}{R_g T_r^2}, \quad \alpha = \frac{(T_r-T_n)}{T_r}, \quad N = \frac{\lambda_s h_v}{(\rho_n u_n c_p)^2}, \quad \Phi = \frac{Y_{Fn}\nu}{Y_{On}}$$

$$\widehat{D}a = \frac{A\ \rho^2\ \lambda_s\ Y_{On}\ T_g^a\ exp(-\beta/\alpha)}{(\rho_n^2\ u_n^2\ c_p)}.$$

The parameter β is the Zel'dovich number, α is the dimensionless heat release, N is the interphase heat transfer parameter, Φ is the equivalence ratio and $\widehat{D}a$ is a modified Damköhler number. The parameter Γ appears dividing the diffusion terms in Eqs. (7) to (9) and it satisfies the condition $\Gamma \gg 1$. By using this property, it is possible to employ the singular perturbation method to find an analytical solution for the problem. In a region of the order of Γ^{-1} near the flame, the gas-phase temperature reaches the flame value, then, since the non-dimensional gas-phase temperature variation is of the order of unity, but the spatial variation is of the order of Γ^{-1}, the description of the pre-heating zone follows a boundary layer method.

5. Outer Zone: problem of the order of unity

In the characteristic length scale $z = \zeta = O(1)$, the diffusive terms are of the order of Γ^{-1} and the reaction is exponentially small. Thus, Eqs. (7) to (10) take the form

$$\varepsilon\frac{dy_F}{d\zeta} = \frac{\varepsilon}{Le_F\ \Gamma}\frac{d^2y_F}{d\zeta^2} \tag{11}$$

$$\varepsilon\frac{dy_O}{d\zeta} = \frac{\varepsilon}{Le_O\ \Gamma}\frac{d^2y_O}{d\zeta^2} \tag{12}$$

$$\varepsilon\frac{d\theta_g}{d\zeta} = \frac{\varepsilon}{\Gamma}\frac{d^2\theta}{d\zeta^2} + N(\theta_s-\theta_g) \tag{13}$$

$$0 = (1-\varepsilon)\frac{d^2\theta_s}{d\zeta^2} - N(\theta_s-\theta_g) \tag{14}$$

The solution of Eqs. (11) to (14) can be written as

$$\begin{array}{rcccl} \theta_s & = & \theta_s^{(0)} & + & \Gamma^{-1}\theta_s^{(0)(1)} + o(\Gamma^{-1}) \\ \theta_g & = & \theta_g^{(0)} & + & \Gamma^{-1}\theta_g^{(0)(1)} + o(\Gamma^{-1}) \\ y_O & = & y_0^{(0)} & + & \Gamma^{-1}y_0^{(0)(1)} + o(\Gamma^{-1}) \\ y_F & = & y_F^{(0)} & + & \Gamma^{-1}y_F^{(0)(1)} + o(\Gamma^{-1}) \end{array} \tag{15}$$

Substituting these expansions in Eqs. (11) to (14) and passing to the limit $\Gamma \to \infty$, the first approximation for the set of equations with order of unity, $O(1)$, is

$$\varepsilon \frac{dy_F^{(0)}}{d\zeta} = 0 \tag{16}$$

$$\varepsilon \frac{dy_O^{(0)}}{d\zeta} = 0 \tag{17}$$

$$\varepsilon \frac{d\theta_g^{(0)}}{d\zeta} = N(\theta_s^{(0)} - \theta_g^{(0)}) \tag{18}$$

$$0 = (1-\varepsilon)\frac{d^2\theta_s^{(0)}}{d\zeta^2} - N(\theta_s^{(0)} - \theta_g^{(0)}) \tag{19}$$

The solution for Eqs. (16) and (17) are $y_F^{(0)} = y_O^{(0)} = 1$, for $\zeta \leq \zeta_f$ and $y_F^{(0)} = 0$ and $y_O^{(0)} = 1 - \Phi$, for $\zeta \geq \zeta_f$. A relation between the gas-phase temperature $\theta_g^{(0)}$ and solid-phase temperature $\theta_s^{(0)}$ is found by combining and integrating Eqs. (18) and (19)

$$\theta_g^{(0)} + \frac{(1-\varepsilon)}{\varepsilon}\frac{d\theta_s^{(0)}}{d\zeta} + D = 0 \tag{20}$$

with $D = 0$ para $\zeta \leq \zeta_f$ e $D = 1$ para $\zeta \geq \zeta_f$.

Taking Eq. (20) into (19)

$$\frac{d^2\theta_s^{(0)}}{d\zeta^2} + \frac{N}{\varepsilon}\frac{d\theta_s^{(0)}}{d\zeta} - \frac{N}{(1-\varepsilon)}\theta_s^{(0)} = -\frac{N}{(1-\varepsilon)}D \tag{21}$$

Once Eq. (21) is solved, the gas-phase temperature $\theta_g^{(0)}$ is determined from Eq. (20). The solution for the solid-phase temperature is given by

$$\theta_s^{(0)} = \begin{cases} \theta_s^{(0)}(\zeta_f)e^{r_1(\zeta-\zeta_f)}, & \text{for} \quad \zeta \leq \zeta_f \\ 1 + (\theta_s^{(0)}(\zeta_f) - 1)e^{-r_2(\zeta-\zeta_f)}, & \text{for} \quad \zeta \geq \zeta_f \end{cases} \tag{22}$$

in which

$$r_1 = -\frac{N}{2\varepsilon} + \frac{1}{2}\left[\left(\frac{N}{\varepsilon}\right)^2 + 4\frac{N}{1-\varepsilon}\right]^{1/2}$$

and

$$r_2 = \frac{N}{2\varepsilon} + \frac{1}{2}\left[\left(\frac{N}{\varepsilon}\right)^2 + 4\frac{N}{1-\varepsilon}\right]^{1/2}$$

The value of the solid-phase temperature at the flame location $\theta_s^{(0)}(\zeta_f)$ is calculated imposing the continuity of the function and its first derivative (the conduction heat flux), obtaining

$$\theta_s^{(0)}(\zeta_f) = \frac{r_2}{r_1 + r_2} = \frac{1}{2} + \frac{1}{2\left\{1 + 4(N/\varepsilon)^{-1}[\varepsilon/(1-\varepsilon)]\right\}^{1/2}} \tag{23}$$

From Eq. (23), we observe that for very low values of porosity, $\varepsilon \ll 1$, the solid-phase temperature at the flame reaches a limiting value equal to unity, $\theta_s^{(0)}(\zeta_f) \to 1$. Conversely, for high porosity, $1 - \varepsilon \ll 1$, the solid-phase temperature at the flame reaches a limiting value equal to 0.5, $\theta_s^{(0)}(\zeta_f) \to 1/2$. Thereby, it is possible to conclude that $1/2 \leq \theta_s^{(0)}(\zeta_f) \leq 1$ for every possible value of porosity.

Once knowing the leading order term of the solid-phase temperature $\theta_s^{(0)}$, the leading order term of the gas-phase temperature $\theta_g^{(0)}$ can be determined from Eq. (20), obtaining

$$\theta_g^{(0)} = \begin{cases} [(1-\varepsilon)/\varepsilon]\ r_1\ \theta_s^{(0)}(\zeta_f)e^{r_1(\zeta-\zeta_f)}, & \text{for} \quad \zeta \leq \zeta_f \\ 1 + [(1-\varepsilon)/\varepsilon]\ r_2\ [1 - \theta_s^{(0)}(\zeta_f)]e^{-r_2(\zeta-\zeta_f)}, & \text{for} \quad \zeta \geq \zeta_f \end{cases} \tag{24}$$

Imposing the condition $\zeta = \zeta_f$ in the solution for the gas-phase temperature, Eq. (24), the following values for the upstream and downstream sides of the flame are found

$$\theta_g^{(0)}(\zeta_f^-) = [(1-\varepsilon)/\varepsilon]\ r_1 \theta_s^{(0)}(\zeta_f) \tag{25}$$

$$\theta_g^{(0+)}(\zeta_f^+) = 1 + [(1-\varepsilon)/\varepsilon]\ r_2\ [1 - \theta_s^{(0)}(\zeta_f)] \tag{26}$$

Subtracting Eq.(25) from (26) and applying the definition of $\theta_s^{(0)}(\zeta_f)$, Eq.(23), the difference $\theta_g^{(0)}(\zeta_f^+) - \theta_g^{(0)}(\zeta_f^-)$ reveals the discontinuity of the gas-phase temperature across the flame in the scale of order of unity, which is

$$\theta_g^{(0)}(\zeta_f^+) - \theta_g^{(0)}(\zeta_f^-) = 1 \tag{27}$$

When the porosity tends to unit, $1 - \varepsilon \ll 1$, the gas-phase solution reduces to a step function across the flame with $\theta_g^{(0)} = 0$, for $\zeta \leq \zeta_f$ and $\theta_g^{(0)} = 1$, for $\zeta \geq \zeta_f$. In the next section, the pre-heating region is analyzed.

6. Inner Zone: problem of the order of Γ^{-1}

In this zone, the variation of the nondimensional variables is of order of unity along a characteristic length of the order of Γ^{-1} around the flame. The solution in this thin zone is denoted by $y_F^{(*)}$, $y_O^{(*)}$, $\theta_g^{(*)}$ and $\theta_s^{(*)}$. The thin region around the flame, defined by the length scale Γ^{-1}, is analyzed imposing the conditions that near the flame, more precisely at $\Gamma(z - \zeta_f) = \xi$, the reactants mass fractions vary according $1 \leq y_F^{(*)} \leq 0$, $1 \leq y_O^{(*)} \leq (1 - \Phi)$ and $\theta_g^{(0)}(\zeta_f^-) \leq \theta_g^{(*)} \leq \theta_g^{(0)}(\zeta_f^+)$. Since there is no chemical source in the energy conservation equation for the solid-phase, the variation of temperature $\theta_s^{(*)}$ is of the order of Γ^{-1}. By rescaling the spatial coordinate to the pre-heating region, the governing equations become

$$\varepsilon \frac{dy_F^{(*)}}{d\xi} = \frac{\varepsilon}{Le_F} \frac{d^2 y_F^{(*)}}{d\xi^2} \tag{28}$$

$$\varepsilon \frac{dy_O^{(*)}}{d\xi} = \frac{\varepsilon}{Le_O} \frac{d^2 y_O^{(*)}}{d\xi^2} \tag{29}$$

$$\varepsilon \frac{d\theta_g^{(*)}}{d\xi} = \varepsilon \frac{d^2 \theta_g^{(*)}}{d\xi^2} + \frac{N}{\Gamma}(\theta_s^{(*)} - \theta_g^{(*)}) \tag{30}$$

$$0 = (1-\varepsilon) \frac{d^2 \theta_s^{(*)}}{d\xi^2} - \frac{N}{\Gamma^2}(\theta_s^{(*)} - \theta_g^{(*)}) \tag{31}$$

The boundary conditions are determined when the solution corresponding to the problem of order of unity is matched with the problem of the order of Γ^{-1}. Thus, in the unburned region (upstream from the flame), for $\xi \to -\infty$, $\theta_g^{(*)} \to \theta_g^{(0)}$, $\theta_s^{(*)} \to \theta_s^{(0)}$ $y_F^{(*)} \to y_F^{(0)} = 1$ and $y_O^{(*)} \to y_O^{(0)} = 1$. In the burned region (downstream the flame), for $\xi \to \infty$, $\theta_g^{(*)} \to \theta_g^{(0)}$, $\theta_s^{(*)} \to \theta_s^{(0)}$ $y_F^{(*)} \to y_F^{(0)} = 0$ and $y_O^{(*)} \to y_O^{(0)} = (1 - \Phi)$.

The solution of Eqs. (28) and (29) are $y_F^{(*)} = 1 - e^{Le_F(\xi - \xi_f)}$ and $y_O^{(*)} = 1 - \Phi e^{Le_O(\xi - \xi_f)}$ for $-\infty \leq \xi \leq \xi_f$, and $y_F^{(*)} = 0$ and $y_O^{(*)} = 1 - \Phi$ for $\xi_f \leq \xi \leq \infty$.

An analysis of Eqs. (30) and (31) reveals that an approximated solution in terms of an expansion on Γ^{-1} can be written as

$$\begin{array}{rclcccl} \theta_s^{(*)} & = & \theta_s^{(*)(0)} & + & \Gamma^{-1}\theta_s^{(*)(1)} & + & \Gamma^{-2}\theta_s^{(*)(1)} \quad +o(\Gamma^{-2}) \\ \theta_g^{(*)} & = & \theta_g^{(*)(0)} & + & \Gamma^{-1}\theta_g^{(*)(1)} & + & \Gamma^{-2}\theta_g^{(*)(1)} \quad +o(\Gamma^{-2}) \end{array} \tag{32}$$

The temperature profiles are determined by the substitution of Eq. (32) into Eqs.(30) and (31). The solution of Eq.(31) is $\theta_s^{(*)(0)} = C^{(*)(0)}$ and $\theta_s^{(*)(1)} = C^{(*)(1)}\xi$, in which the value of $C^{(*)(0)}$ and $C^{(*)(1)}$ are determined matching the solution $\theta_s^{(*)}$ with $\theta_s^{(0)}$. The matching implies that, for $\xi \to -\infty$, the function must be continuous and the heat flux in the solid-phase $d\theta_s^{(*)}/d\xi$ is equal to the heat flux $d\theta_s^{(0)}/d\zeta$ at $\zeta = \zeta_f$. Then, $C^{(*)(0)} = \theta_s^{(0)}(\zeta_f)$ and $C^{(*)(1)} = d\theta_s^{(0)}/d\zeta|_{\zeta=\zeta_f}$.

The equation for the leading order of the gas-phase, $\theta_g^{(*)(0)}$, is given by

$$\varepsilon \frac{d\theta_g^{(*)(0)}}{d\xi} = \varepsilon \frac{d^2\theta_g^{(*)(0)}}{d\xi^2} \tag{33}$$

whose solution is $\theta_g^{(*)(0)}(\xi) = C_3^{(*)} e^{\xi} + C_4^{(*)}$. The constants are determined by the matching with the profile of $\theta_g^{(0)}$ at $\zeta = \zeta_f$. Thus, as $\xi \to -\infty$, $\theta_g^{(*)(0)} \to \theta_g^{(0)}(\zeta_f^-)$ leading to $\theta_g^{(*)(0)}(\xi) = C_3^{(*)} e^{\xi} + \theta_g^{(0)}(\zeta_f^-)$. The value of $C_3^{(*)}$ is specified applying the condition at the flame, $\theta_g^{(*)(0)}(\xi = 0) = \theta_g^{(0)}(\zeta_f^+)$, since downstream from the flame there is the region controlled by the interfacial heat transfer from the gas to the solid-phase. Then, recalling that $\theta_g^{(0)}(\zeta_f^-) - \theta_g^{(0)}(\zeta_f^+) = 1$, we have

$$\theta_g^{(*)(0)}(\xi) = \theta_g^{(0)}(\zeta_f^-) + e^{(\xi - \xi_f)} \tag{34}$$

The $O(\Gamma^{-1})$ correction for the gas temperature inside the preheating region $\theta_g^{(*)(1)}$ is given by

$$\frac{d}{d\xi}\left(e^{-\xi} \frac{d}{d\xi} \theta_g^{(*)(1)} \right) = \frac{N}{\varepsilon} \left\{ 1 + [\theta_g^{(0)}(\zeta_f^-) - \theta_s^{(0)}(\zeta_f)] e^{-\xi} \right\} \tag{35}$$

whose solution is:

$$\theta_g^{(*)(1)} = \frac{N}{\varepsilon} \left\{ (\xi e^{\xi} - e^{\xi} + 1) + [\theta_s^{(0)}(\zeta_f) - \theta_g^{(0)}(\zeta_f^-)] \xi \right\} \tag{36}$$

after imposing the condition $\theta_g^{(*)(1)} = 0$ at $\xi = 0$ and the matching condition $d\theta_g^{(*)(1)}/d\xi \to d\theta_g^{(0)}/d\zeta \Big|_{\zeta_f}$.

7. Inner zone: reaction region

The description of the reaction zone follows (Liñán, 1974), which demands

$$\begin{array}{lcllll} \theta_s & = & \theta_{sf}^{(*)} & + & \delta\ \theta_s^{(1)} & +o(\delta) \\ \theta_g & = & \theta_{gf}^{(*)} & - & \delta\ (\theta_g^{(1)} + m\eta + p) & +o(\delta) \\ y_O & = & y_{0f}^{(*)} & + & \delta\ d_O\, Le_O\, y_O^{(1)} & +o(\delta) \\ y_F & = & 0 & + & \delta\ d_F\, Le_F\, y_F^{(1)}/\gamma & +o(\delta) \\ z & = & \bar{\zeta}_f & + & \delta\ \Gamma^{-1}\ (\eta + p/m)/\gamma & +o(\delta) \end{array} \tag{37}$$

in which $\bar{\zeta}_f = \zeta_f + \Gamma^{-1}\xi_f$ and $y_{0f}^{(*)} = 1 - \Phi$.

Substituting the solution (37) into the conservation equations (7) to (10), the description of the reaction zone is governed by

$$\frac{d^2 y_F^{(1)}}{d\eta^2} = \bar{Da}\ y_F^{(1)}\ \exp[-(\theta_g^{(1)} + m\eta + p)] \tag{38}$$

$$\frac{d^2 y_O^{(1)}}{d\eta^2} = \frac{\nu d_F}{\gamma d_O} \bar{Da}\ y_F^{(1)}\ \exp[-(\theta_g^{(1)} + m\eta + p)] \tag{39}$$

$$\varepsilon \frac{d^2\theta_g^{(1)}}{d\eta^2} = \varepsilon \frac{d_F}{\gamma} \bar{Da}\ y_F^{(1)}\ \exp[-(\theta_g^{(1)} + m\eta + p) + \frac{\delta N}{\gamma^2 \Gamma}(\theta_s^{(*)} - \theta_g^{(*)}) \tag{40}$$

$$0 = (1 - \varepsilon) \frac{d^2\theta_s^{(1)}}{d\eta^2} - \frac{\delta N}{\gamma^2 \Gamma}(\theta_s^{(*)} - \theta_g^{(*)}) \tag{41}$$

in which

$$\bar{Da} = \frac{\widehat{Da}}{\Gamma} \left(\frac{\delta^2 Le_F (1 - \Phi)}{\gamma^2} \right) \exp\left\{ \frac{-\beta(1 - \theta_{gf}^{(*)})}{[1 - \alpha(1 - \theta_{gf}^{(*)})]} \right\},$$

We note that the term $\Gamma^{-1}\widehat{Da}$ recovers the free-flame Damköhler definition. In the characteristic length scale of the order of $\delta\Gamma^{-1}$, the heat transfer from the gas-phase to the solid-phase is negligible ($\delta N/\gamma^2\Gamma \ll 1$) compared to the heat transfer in the solid-phase from the equilibrium zone to the frozen zone. Therefore,

$\theta_s^{(1)} = C^{(1)}\eta$ and from the energy conservation $C^{(1)} = C^{(*)}$.

An analysis of the system of equations (38) to (41) leads to the choice $\gamma = d_F$ and $p = ln(2\bar{D}a)$. Then, this system of equations can be written as

$$\frac{d_O}{\nu}\frac{d^2 y_O^{(1)}}{d\eta^2} = \frac{d^2 y_F^{(1)}}{d\eta^2} = \frac{d^2\theta_g^{(1)}}{d\eta^2} = \frac{1}{2}\, y_F^{(1)}\ \exp[-(\theta_g^{(1)} + m\eta)] \tag{42}$$

The mass fluxes d_F and d_O are defined for the upstream side as

$$-\frac{1}{Le_F}\frac{dy_F^{(*)}}{d\xi}\bigg|_{\xi_f^-} = d_F, \qquad \frac{1}{Le_O}\frac{dy_O^{(*)}}{d\xi}\bigg|_{\xi_f^-} = d_O$$

and for the downstream side as

$$\frac{1}{Le_F}\frac{dy_F^{(*)}}{d\xi}\bigg|_{\xi_f^+} = 0, \qquad \frac{1}{Le_O}\frac{dy_O^{(*)}}{d\xi}\bigg|_{\xi_f^+} = 0$$

The heat flux at both sides of the flame, d_θ^- and d_θ^+ are defined as

$$\frac{d\theta_g^{(*)}}{d\xi}\bigg|_{\xi_f^-} = d_\theta^- \quad \text{and} \quad \frac{d\theta_g^{(*)}}{d\xi}\bigg|_{\xi_f^+} = -d_\theta^+$$

Since the solution $(\ )^{(1)}$ has to match with the solution $(\ )^{(*)}$, then, as $\eta \to -\infty$,

$$\frac{dy_F^{(1)}}{d\eta} = -1, \qquad \frac{dy_O^{(1)}}{d\eta} = -1/\gamma, \qquad \text{and} \qquad \frac{d(\theta_g^{(1)} + m\eta)}{d\eta} = -d_\theta^-/\gamma \tag{43}$$

and as $\eta \to \infty$,

$$\frac{dy_F^{(1)}}{d\eta} = 0, \qquad \frac{dy_O^{(0)}}{d\eta} = 0 \qquad \text{and} \qquad \frac{d(\theta_g^{(1)} + m\eta)}{d\eta} = d_\theta^+/\gamma \tag{44}$$

By choosing appropriately the value of $m = d_\theta^+/\gamma$, the heat flux is normalized

$$\frac{d\theta_g^{(1)}}{d\eta}\bigg|_{\eta\to-\infty} = -1 \quad \text{and} \quad \frac{d\theta_g^{(1)}}{d\eta}\bigg|_{\eta\to\infty} = 0 \tag{45}$$

From the conservation of energy at the flame $d_\theta^+ + d_\theta^- = d_F = \gamma$, then $m = d_\theta^+/(d_\theta^+ + d_\theta^-)$.

Combining Eqs. (42), and applying the boundary conditions Eqs. (43) to (45), we obtain $\theta_g^{(1)} = y_F^{(1)}$. Thus, the problem in the reaction region reduces to find the solution of

$$\frac{d^2 y_F^{(1)}}{d\eta^2} = \frac{1}{2}\, y_F^{(1)}\ \exp[-(y_F^{(1)} + m\eta)] \tag{46}$$

From Eq. (43), it is observed that

$$n = \lim_{\eta\to-\infty}(y_F^{(1)} - \eta)$$

The displacement n is equal to $-p/m$, then

$$\frac{2A\rho_f^2\lambda_s Y_{On} T_{gf}^a\ exp(-\beta/\alpha)}{(\rho_n^2\ s_f^2\ c_p)}\ \left(\frac{\delta^2 Le_F(1-\Phi)}{d_F^2\,\Gamma}\right)\ \exp\left\{\frac{-\beta(1-\theta_{gf}^{(*)})}{[1-\alpha(1-\theta_{gf}^{(*)})]}\right\} = e^{-m\,n} \tag{47}$$

in which

$$m\,n = 1.344m - 4m^2(1-m)/(1-2m) + 3m^3 - ln(1-4m^2), \quad \text{for} \quad -0.2 < m < 0.5 \tag{48}$$

Equation (47) provides a first-order estimate for the flame speed. Note that in combustion within a porous-medium, the value of m is bounded by $0 \le m \le 0.5$. The limit $m = 0$ corresponds to a situation in which the flame temperature is equal to the equilibrium adiabatic temperature. Under this circumstance, there is no

excess enthalpy. Thus, the excess of enthalpy requires $m > 0$. The limit $m = 0.5$ corresponds to a situation in which the heat loss to the equilibrium zone is equal to that to the frozen zone and under this condition the flame is not stable, i.e., there is extinction. Equation (48) is a approximation of the numerical solution of Eq. (46) with the boundary conditions given by Eqs.(43) and (44) - see Liñán (1974) for details. The value of m can be found from

$$m = \frac{\left[(1-\varepsilon)/\varepsilon\right] r_2^2 \Gamma^{-1} \left(1 - \theta_s^{(0)}(\zeta_f)\right)}{1 + \left[(1-\varepsilon)/\varepsilon\right] r_2^2 \Gamma^{-1} \left(1 - \theta_s^{(0)}(\zeta_f)\right)} \tag{49}$$

8. Discussion

For brevity, the discussion is restricted to $Le = 1$, since the effect of the gas Lewis number in a laminar flame is presented elsewhere (Law and Sung, 2000; Wichman and Vance, 1997). The reaction rate parameters were adjusted to give a reasonable agreement with experimental results for free flames with equivalence ratio ranging from 0.6 to 0.9 (Zhu et al., 1988). The mean pore diameter is modeled as $d_m = \left(\sqrt{4\varepsilon/\pi}\right) / (39.37\ PPI)$, which is a uniform pore distribution model, where PPI stands for pores per inch. The volumetric heat transfer coefficient h_v is modeled following Fu et al. (1998) which uses a volumetric Nusselt number $Nu_v = C' \,\mathrm{Re}^{m'}$, where $Nu_v = h_v d_m^2/\lambda_g$ and Re is the Reynolds number, $\mathrm{Re} = \rho_n u_n d_m/\mu_n$.

Table 1 shows thermodynamic, transport and geometric properties of the solid and gas-phases typical of porous burners (Catapan et al., 2005; Mösβauer et al.,1999). It is also shown the parameters used in the coputations and some results for $\phi = 0.8$, $\Gamma = 60$ and $\varepsilon = 0.8$.

Table 1. Thermodynamic, transport and geometric properties for the solid and gas (methane/air) phases and the corresponding non-dimensional parameters.

Gas-Phase Properties				Solid-Phase Properties				Nondimensionals	
R	8.314	J/mol-K		λ_s	4.92	W/m-K		Nu_v	18.85
c_p	1452	J/kg-K		PPI	10	ppi		Re	54.33
λ_g	0.082	W/m-K		ε	0.8			α	0.84
E	1.77×10^5	J/mol		d_m	2.5×10^{-3}	m		β	9.7
A	6.93×10^{12}	m^3/kg-s		C'	0.252			Γ	60
a	0			m'	1.08			N	0.6
Q	5.014×10^7	J/kg		h_v	2.35×10^5	W/m^3-K		$\widehat{Da}$	1286
μ_n	4.5×10^{-5}	kg/m-s						$\overline{Da}$	0.495
T_n	298	K						m	7.55×10^{-3}
T_r	1832	K						n	1.366
T_{gf}	2157	K						Le	1
s_f	0.833	m/s						Φ	0.8

Figure (2) shows the flame structure for $\Phi = 0.8$, $\Gamma = 60$ and $\varepsilon = 0.8$ as a function of the space coordinate ξ. The range used for the spatial scale represents the solution of the problem of $O(1)$, in which the solid conduction and the interphase heat transfer are the dominant phenomenons. The flame can be seen as a sheet where the fuel and gas profiles are discontinuous. For these conditions the gas temperature exceeds the adiabatic limit in 20%, which corresponds to the gas preheat just upstream of the flame.

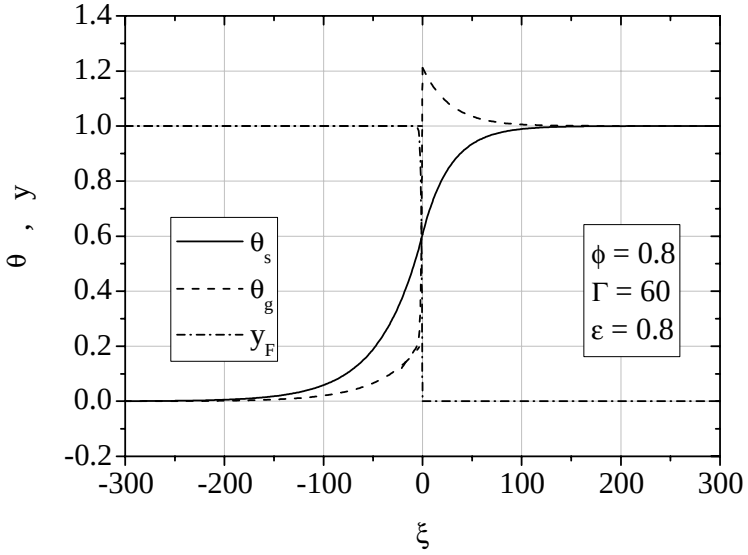

Figure 2 - Nondimensional gas and solid temperatures and fuel fraction profile for a flame with $\Phi = 0.8$, $\Gamma = 60$ and $\varepsilon = 0.8$ (solution of the $O(1)$ problem).

Figure (3) shows the same result as Fig.(2) with a range for the spatial scale that represents the solution of the problem of $O(\Gamma^{-1})$. It is possible to see the solution in the preheating region connecting the discontinuous profiles of $\theta_g^{(0)}$ and $y_F^{(0)}$ across the flame. Close to the reaction sheet, where the gas-phase temperature and fuel mass fraction slopes are discontinuous, the thermal diffusion in the gas-phase becomes the dominant phenomenon. Comparing Figs. (2) and (3) it is seen that the thermal affected region (l_{Ds}) is about 40 times larger than the preheating region (l_{Dg}) as a result of the high thermal conductivity of the solid matrix.

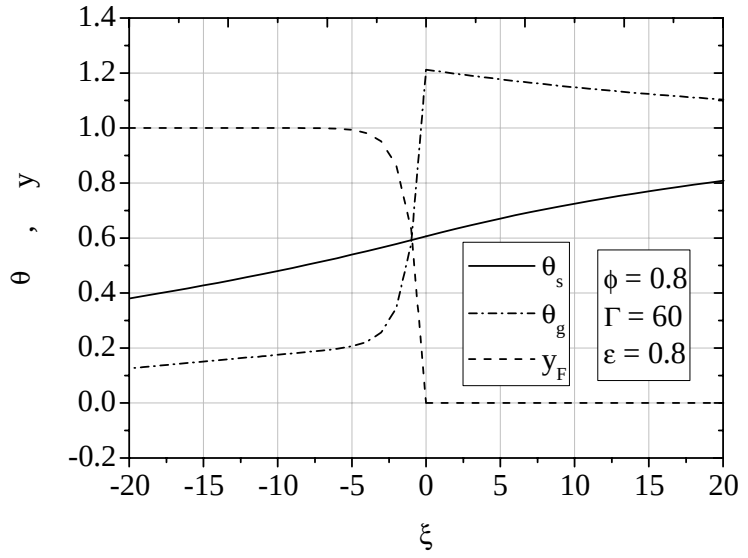

Figure 3 - Nondimensional gas and solid temperatures and fuel fraction profile for a flame with $\Phi = 0.8$, $\Gamma = 60$ and $\varepsilon = 0.8$ (solution of the $O(\Gamma^{-1})$ problem).

Figure (4) shows the effect of the thermal conductivities ratio, Γ, on the maximum nondimensional gas temperature at the flame $[\theta_{g,f} = \theta_g^{(0)}(\zeta_f^+)]$, on the nondimensional solid temperature at the flame $[\theta_{s,f} = \theta_s^{(0)}(\zeta_f)]$ and on the flame velocity (s_f) for $\varepsilon = 0.8$ and equivalence ratios ranging from 0.6 to 0.9. It is important to note that the model is not valid for equivalence ratios near unity because in this case the oxidant concentration $(1 - \Phi)$ in Eq. (47) tends to zero and prevails over the thermal effect. In order to reach the stoichiometric mixture it would be necessary to solve the $y_o^{(1)}$ correction.

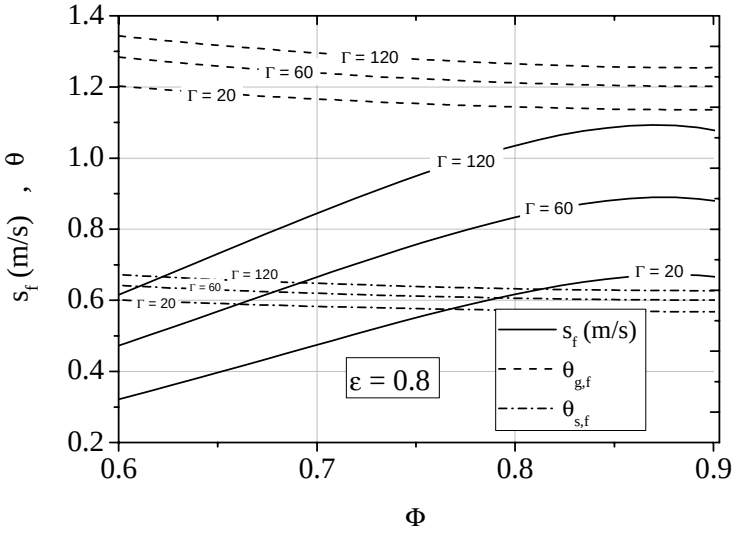

Figure 4 - Effect of the thermal conductivity ratio, Γ, on the maximum gas temperature at the flame ($\theta_{g,f}$), on the solid temperature at the flame ($\theta_{s,f}$) and on the flame velocity (s_f) for equivalence rations ranging from 0.5 to 0.9 and $\varepsilon = 0.8$.

The flame velocity, s_f, increases with Φ and Γ, reaching values above that of an adiabatic free flame, that is about 0,4 m/s for a stoichiometric methane-air mixture. The superadiabatic effect is more pronounced for leaner mixtures, where the maximum gas-phase temperature reaches values 35% above the adiabatic flame temperature for the inlet conditions ($\theta_{g,f} = 1,35$ for $\Phi = 0.6$). The solid-phase temperature at the flame varies in the range of 0.57 to 0.67, in accordance with the limits $1/2 < \theta_{g,f} < 1$, stated by Eq.(23).

Figure (5) shows the interphase heat transfer parameter N as a function of Φ and Γ for $\varepsilon = 0.8$. For any Γ, the heat transfer parameter decreases as Φ increases. This can be understood by recalling that N is proportional to $1/s_f^2$ ($s_f = u_n$ for a stationary flames) and that higher flame velocities are found for higher equivalence ratios. The higher flame velocities also increase the volumetric heat transfer coefficient h_v, but this effect is counterbalanced by the reduced time to exchange heat. Figure (6) shows the flame velocity nondimensionalized by the adiabatic free flame velocity s_{ad}^0 (obtained when $\varepsilon = 1$). The results show again higher nondimensional flame velocities for leaner mixtures ($s_f / s_{ad}^0 \sim 6$ for $\Phi = 0.6$ and $\Gamma = 120$) as a result of the higher heat transfer parameter. The superadiabatic effect is a function of the heat recirculation, then it tends to be more pronounced for higher values of N and Γ, i.e., for leaner mixtures and higher solid thermal conductivities.

The model fails for lower equivalence ratios ($\Phi < 0.6$) due to the increase in the heat transfer parameter N. In theses cases the connection between the solutions in the gas and solid length scales is very poor. This happens because the interphase heat transfer in the preheating region has been neglect in the present model, but it becomes relevant for lower equivalence ratios.

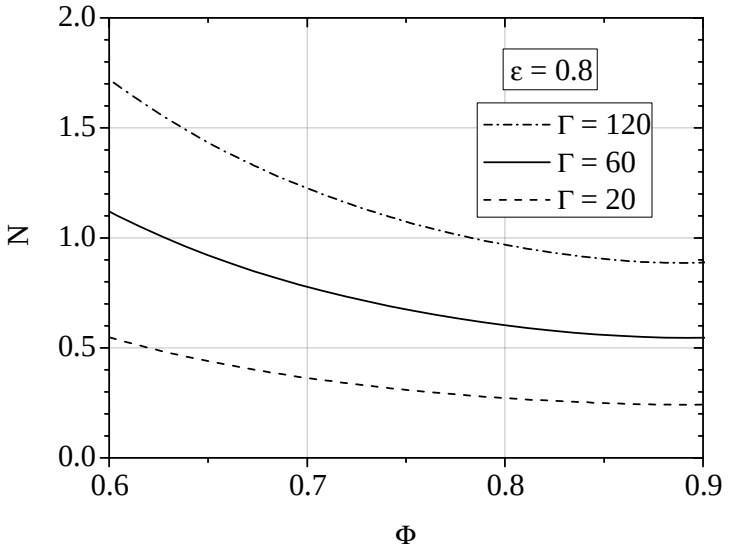

Figure 5 - Intraphase heat transfer parameter N as a function Φ and Γ for $\varepsilon = 0.8$.

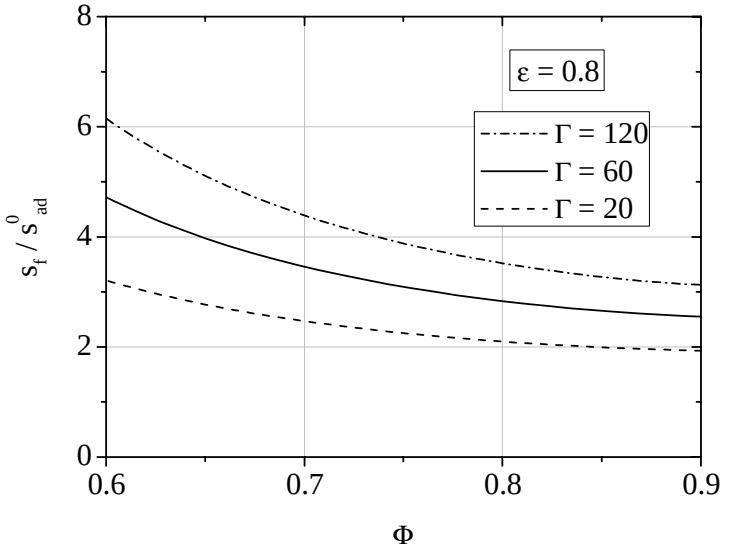

Figure 6 - Flame nondimensionalized by the adiabatic free flame velocity u_{ad} as a function Φ and Γ for $\varepsilon = 0.8$.

Figure (7) shows the effect of the porosity on the temperature of the solid and gas phases at the flame, $\theta_{g,f}$ and $\theta_{s,f}$, and on the dimensional flame velocity, s_f, for $\Gamma = 60$. The superadiabatic effect is amplified as the porosity is decreased because more heat is recirculated by the solid-phase. When $\varepsilon = 1$ the model tends to the free flame solution, i.e., $\theta_{g,f}$ is unity over the entire range of Φ and s_f reduces to s^0_{ad}. For this limiting case $\theta_{s,f}$ is 0.5, its lower value according to Eq.(23), nevertheless in this limit the solid temperature is meaningless since there is no interphasic heat exchange. Figure (8) shows the dependence of N, $\theta_{g,f}$, $\theta_{s,f}$ and $s_f\,/s_{ad}$ on the volumetric porosity for $\Phi = 0.8$ and $\Gamma = 60$. The heat exchange parameter N decreases as the porosity is decreased, but at the same time the effect of the solid-phase becomes more important since there is more solid-phase in the matrix. The result is that decreasing ε larger amounts of heat are transported by the solid matrix and even for lower values of N the heat recirculated is higher.

Therefore, the superadiabatic effect is mainly a function of three parameters: the matrix porosity ε, the conductivities ratio Γ, that together account for the transport of heat by the solid-phase, and the heat exchange parameter N, that accounts for the heat transfer between the solid-phase and the gas-phase. The combinations among these three parameters will define the heat recirculation induced by the matrix and consequently the superadiabatic effect.

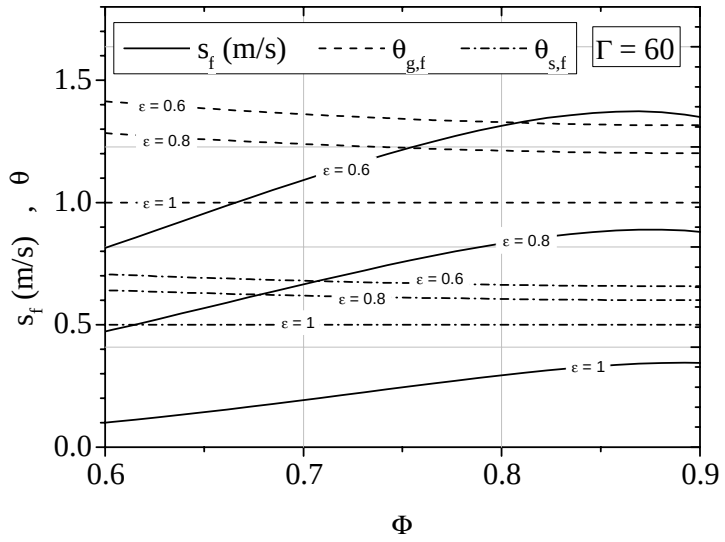

Figure 7 - Effect of the porosity on the temperatures $\theta_{g,f}$ and $\theta_{s,f}$ and on the flame velocity for $\Gamma = 60$.

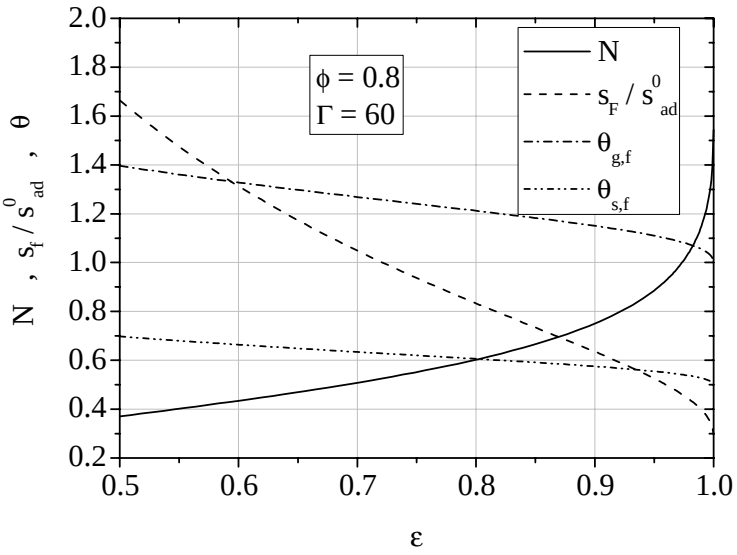

Figure 8 - Dependence of N, $\theta_{g,f}$, $\theta_{s,f}$ and s_f/s_{ad}^0 with the volumetric porosity for $\Phi = 0.8$ and $\Gamma = 60$.

9. Conclusions

This work presented an asymptotic solution for an infinite, adiabatic porous burner considering three different characteristic length scales: the solid-phase diffusion length scale (l_{Ds}), where the solid-phase heat conduction and interphase heat transfer dominate the problem, the gas-phase diffusion length scale (l_{Dg}), where the gas-phase convection and heat conduction dominate the problem, and the reaction length scale (l_R), where reaction and gas-phase heat conduction dominate the problem. Explicit solutions for the gas and solid temperatures and for the fuel consumption were found as functions of the problem parameters for the l_{Ds} and l_{Dg} characteristic length scales. The reaction length scale was used to find an expression for the flame velocity.

The results showed that the influence of the porous medium on the flame is to increase its temperature and velocity and that this effect is more pronounced for leaner mixtures, higher thermal conductivities ratios and lower porosities. The thermal affected region (l_{Ds}) is about 40 times larger than the preheating region (l_{Dg}) as a result of the high thermal conductivity of the solid matrix. Maximum gas-phase temperatures up to 40% above the corresponding adiabatic free-flame temperature and flame velocities up to 12 times the corresponding adiabatic free-flame velocity are found in the range of analysis.

The results showed that the superadiabatic effect is a function of three main parameters: the matrix porosity ε and the conductivities ratio Γ, that together account for the transport of heat by the solid-phase, and the heat exchange parameter N, that accounts for the heat transfer between the solid-phase and the gas-phase. The combinations among these three parameters will define the heat recirculation induced by the matrix and consequently the superadiabatic effect. For a higher superadiabatic effect it is desired to have low porosity ε, high thermal conductivities ratio Γ and to operate with fuel lean mixtures. A way to increase the effective solid thermal conductivity is to work with a medium with thick solid characteristic particle size.

Due to the simplifications assumed by the model the solution fails for lower equivalence ratios ($\Phi < 0.6$) and for equivalence ratios near unity.

10. References

Barra, A. J. e Ellzey, J. L.,2004, "Heat recirculation and heat transfer in porous burners", Combustion and Flame, v. 137, p. 230-241.

Echigo, R., 1991, "Radiation enhanced/controlled phenomena of heat and mass transfer in porous media", ASME/JSME Thermal Engineering Proceedings, Vol.4, pp. 21-32.

Catapan, R.C., Pereira, F.M. and Oliveira, A.A.M., 2005, "Development of a radiant porous burner with a combined thermal and fluidynamic mechanism of flame stabilization", Proceedings of the 18th Congress of Mechanical Engineering, Ouro Preto.

Fu, x., Viskanta, R. and Gore, J.P., 1998, "Measurement and correlation of volumetric heat transfer coefficients of cellular ceramics", Experimental Thermal and Fluid science, Vol.17, pp. 285-293.

Howell, J.R., Hall, M.J. and Ellzey, J.L., 1996, "Combustion of hydrocarbon fuels within porous inert media", Progress in Energy and Combustion Science, Vol.22, pp. 121-145.

Law, C.K. and Sung, C.J., 2000, "Structure, aerodynamics and geometry of premixed flamelets", Progress in Energy and Combustion Science, Vol.26, pp. 459-505.

Liñán, A., 1973, "The asymptotic structure of the counterflow diffusion flames for large activation energies", Acta Astronautica, Vol.1, pp.1007-1039.

McIntosh, A.C., and Prothero, A., 1991, "A model of large heat transfer surface combustion with radiant heat emission", Combustion and Flame, Vol.83, pp.111-126.

Mösβauer, S., Pickenäcker, O., Pickenäcker K. and Trimis, D., 1999, "Application of the porous burner technology in energy- and heat-engineering", V International Conference on Technologies for a Clean Air Environment, Lisbon.

Pereira, F.M. and Oliveira, A.A.M., 2005, "Analytical study of the excess enthalpy in the combustion within porous media", Proceedings of the 18th Congress of Mechanical Engineering, Ouro Preto.

Pereira, F.M. and Oliveira, A.A.M., 2002, "Medição dos limites de estabilidade de chamas pré-misturadas de metano e ar em meios porosos de esponja cerâmica", IX Brazilian Congress of Thermal Engineering and Sciences, Caxambu.

Oliveira, A.A.M. and Kaviany, M., 2001, "Nonequilibrium in the transport of heat and reactants in combustion in porous media", Progress in Energy and Combustion Science, Vol.27, pp. 523-545.

Saharaoui, M. and Kaviany, M., 1994, "Direct Simulation vs Volume-Averaged Treatment of Adiabatic, Premixed Flame in a Porous Medium, 2001, "International Journal of Heat and Mass Transfer, Vol.17, No.18, pp. 2817-2834.

Wichman, I.S. and Vance, R., 1997, "A Study of one-dimensional laminar premixed flame annihilation", Combustion and Flame, Vol.110, pp. 508-523.

Williams, F., 1985, "Combustion theory the fundamental theory of chemically reacting flow systems", Perseus Publishing; 2nd edition.

Zel'doich, Ya. B.; Barenblatt, G. L., Librovich, V. B. and Makhviladze, G. M., 1985, "The mathematical theory of combustion and explosions", Consultants Bureau, New York

Zhu D. L., Egolfopoulos F. N. and Law C. K., 1988, "Experimental and numerical determination of laminar flame speeds of methane/(Ar, N2, CO2)-Air mixtures as function of stoichiometry, pressure and flame temperature", 22th Symposium on Combustion/The Combustion Institute, pp. 1537-1545.